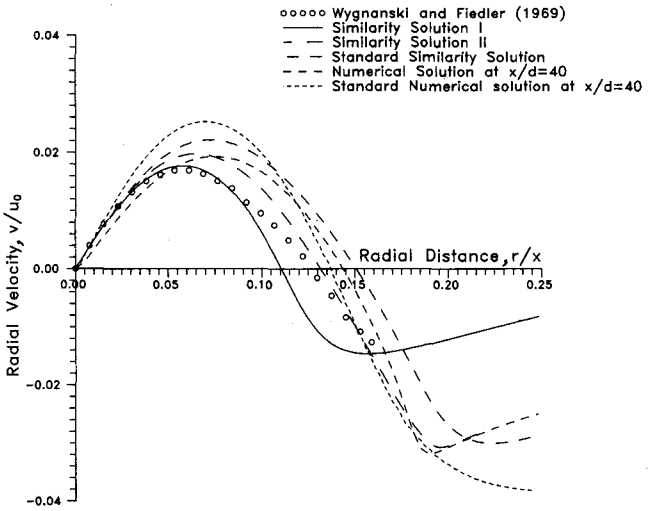

Fig. 3 Radial velocity, v/u_0, obtained with the optimized turbulence model

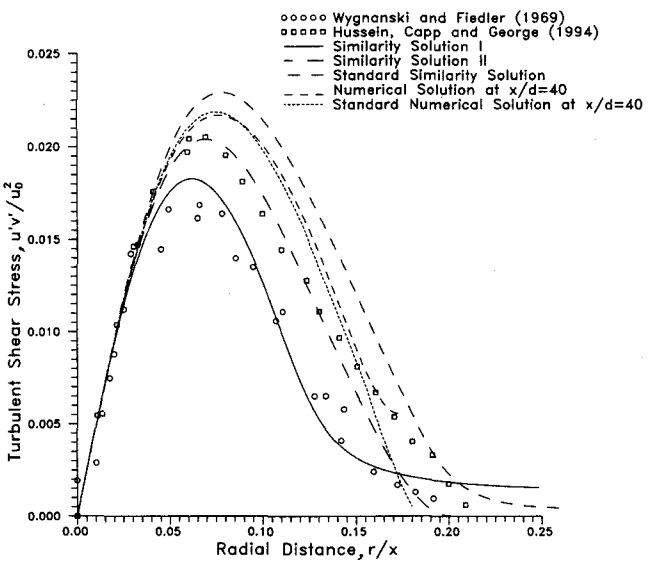

Fig. 4 Radial distribution of turbulent shear stress, $u'v'/u_0^2$, obtained with the optimized turbulence model

data of Hussein et al., 1994, up to $r/x = 0.18$. At the edge of the jet, the results are mixed and any agreement with the similarity or the numerical solutions appears to be coincidental.

The radial profiles of the turbulent shear stress are shown in Fig. 4. The shear stress results of similarity solution I show a close agreement to the experimental data of Wygnanski and Fiedler at the core of the jet as well as in the far field, up to a radial distance $r/x = 0.2$. The similarity solution II agrees better with the experimental data of Hussein et al. (1994).

IV Conclusions

A similarity method has been developed to transform the partial differential equations of a round axisymmetric jet onto ordinary differential equations. The k-ϵ turbulence model equations are also transformed. The results obtained from the optimized similarity solutions agree well with available experimental data of the velocity and the shear stress profiles.

Acknowledgments

The authors are grateful for the partial support provided for this work by grants from NASA, LEQSF, and DOE (through CBR) to Tulane University.

References

Abramovich, G. N., 1963, *The Theory of Turbulent Jets,* MIT Press, Cambridge MA.

George, W. K., 1989, "The Self-Preservation of Turbulent Flows and its Relation to Initial Conditions and Coherent Structures," *Advances in Turbulence,* W. K. George and R.E.A. Arndt, eds., Hemisphere, pp. 39–72.

Hussein J. H., Capp, S. P., and George, W. K., 1994, "Velocity Measurements in a High-Reynolds-Number, Momentum Conserving, Axisymmetric, Turbulent Jet," *Journal of Fluid Mechanics,* Vol. 258, pp. 31–75.

Kumar, S., Nikitopoulos, D. N., and Michaelides, E. E., 1989, "The Effect of Bubbles on the Turbulence of a Liquid Jet," *Experiments in Fluids,* Vol. 7, pp. 484–492.

List, E. J., 1982, *Mechanics of Turbulent Buoyant Jets and Plumes in Turbulent buoyant Jets and Plumes,* W. Rodi, ed., Pergamon Press, Oxford.

Paullay, A. J., Melnik, R. E., Rubel, A., Rudman, S., and Siclari, M. J., 1985, "Similarity Solution for Plane and Radial Jets Using a k-ϵ Turbulent Model," ASME JOURNAL OF FLUIDS ENGINEERING, Vol. 107, pp. 79–85.

So, R. M. C., 1986, "On Similarity Solutions for Turbulent and Heated Round Jets," *ZAMP,* Vol. 37, pp. 625–631.

Townsend, A. A., 1976, *The Structure of Turbulent Shear Flow,* Cambridge Univ. Press.

Wollmers, H. and Rotta, J. C., 1977, "Similar Solutions of the Mean Velocity, Turbulent Energy and Length Scale Equations," *AIAA Journal,* Vol. 15, No. 5, pp. 714–720.

Wygnanski, I. and Fiedler, H. E., 1969, "Some Measurements in the Self-Preserving Jet," *Journal of Fluid Mechanics,* Vol. 38, pp. 577–612.

Flow Measurements Near a Reynolds Ridge

A. Warncke,[1] M. Gharib,[1] and T. Roesgen[2]

Introduction

The Reynolds ridge is a well-known phenomenon first observed in 1854 by Henry David Thoreau. It was then rediscovered by Langton in 1872, but Reynolds was the first to recognize that the surface tension difference was the physical mechanism behind its formation and saw the equality between the case of a spreading film and that of a stagnant film met by oncoming flow. However, it wasn't until McCutchen in 1970 that the prediction of a boundary layer forming beneath the film was introduced as the cause of the surface deformation rise ahead of the film due to the retardation of the flow. The first quantitative theory of the ridge was formed by Harper and Dixon (1974), who stated that the surface tension gradient balances the viscous shear stress generated in the boundary layer. Experimental studies of the ridge so far include Schlieren visualizations by Sellin (1968) as well as by Scott (1982) who measured the surface slope across the ridge and found good comparisons between the theoretical results of Harper and Dixon. Finally, it was Scott who recognized that even at very low levels of surface contamination the Reynolds ridge is found to exist.

The more recent interest in the study of the Reynolds ridge is its application to studying flows on the ocean surface. Naturally occurring soluble and insoluble surfactants abound on the ocean surface. Thus, a study of the effect of surfactant gradients and the consequent production of vorticity in the vicinity of a Reynolds ridge, can provide insight into the overall understanding of the air/water interface of the ocean surface.

[1] Graduate Aeronautical Laboratories, California Institute of Technology, Pasadena, CA 91125.

[2] Section WGO ESA-ESTEC, Postbus 299 Keplerlan 1 NL-2200 AG, Noordwijk, Netherlands.

Contributed by the Fluids Engineering Division of THE AMERICAN SOCIETY OF MECHANICAL ENGINEERS. Manuscript received by the Fluids Engineering Division September 12, 1995; revised manuscript received April 16, 1996. Associate Technical Editor: D. P. Telionis.

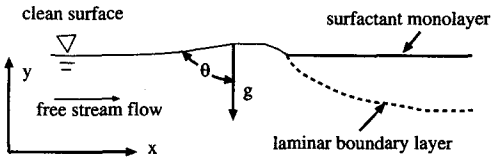

Fig. 1 Flow schematic near a Reynolds ridge

Theory

The equation for surface parallel vorticity, as derived from Lugt (1987, 1988), Lundgren (1988), and shown by Gharib and Weigand (1995), in a two-dimensional curvilinear coordinate system is:

$$\omega_z = -\frac{\tau_{\text{Air}}}{\mu} - \frac{1}{\mu}\frac{\partial \sigma}{\partial s} - 2\frac{u_s}{R} + 2\frac{\partial u_r}{\partial s} \qquad (1)$$

where s is the surface tangential coordinate, r is the surface normal coordinate, z is the coordinate normal to the two dimensional plane defined by r and s, R is the radius of curvature of the free surface, σ is the surface tension, and the shear force due to air is included but most often assumed negligible. From this equation it is obvious that the surface tension gradient plays an important role in the boundary condition at an interface. It will be shown how this boundary condition results in a vorticity flux at the free surface.

So far, as stated above, it is understood that the physical mechanism for the free surface elevation at the leading edge of a surfactant monolayer is due to the retardation of flow within the boundary layer beneath the film. However, this deceleration of the flow ahead of the film, due to the presence of a surface tension gradient, provides a source of vorticity at the free surface. For the case experimentally tested, the Reynolds ridge is stationary in front of a stagnant film met by oncoming flow (see Fig. 1). (Note in Fig. 1 x and y are defined as the surface parallel and normal coordinates respectively to correspond with the presentation of the results.) For this steady-state case, where the normal component of velocity at the free surface is inherently zero and the pressure at the free surface is constant, the equation for the vorticity flux at a free surface as derived by Rood (1995) and Gharib (1992) simplifies to:

$$v\left(\frac{\partial \omega_z}{\partial r}\right)_{r=0} \cong -u_s\frac{\partial u_s}{\partial s} - g\cos\theta \qquad (2)$$

such that θ is the angle between the free surface and g, the direction of gravity. Thus a positive value of the right hand side implies a positive flux of positive vorticity into the flow at the free surface. Also, for this case, it is obvious that the vorticity flux at the free surface can be attributed to two sources: (1) the deceleration of the flow at the free surface and (2) the local slope of the free surface due to a change of θ from ninety degrees. Thus, experimentally measuring these quantities will indicate the dominating source of vorticity generated at the free surface in the presence of a Reynolds ridge.

Experimental Setup

A small free surface water tunnel with a 4 in. × 4 in. × 12-in. long test section, as shown in Fig. 2, was constructed to provide the formation of a Reynolds ridge for experimental study. For the results presented, Sodium Dodecyl Sulfate (SDS), a soluble surfactant, was used as a surface contaminant to form the surfactant monolayer behind the Reynolds ridge. First, the surface slope was measured using a new technique developed by Roesgen (1996). In short, it involves measuring the displacement of collimated light, as it travels from below the free surface, through the use of an array of microlenses. By

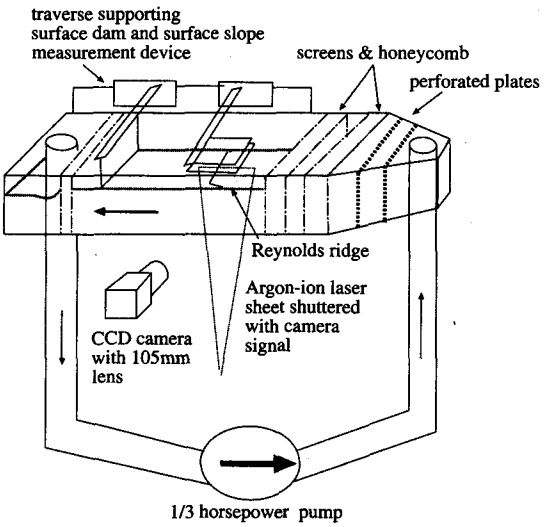

Fig. 2 Experimental setup

imaging the focal plane of the lenslet array and measuring the displacement of the focal points, one can measure the slope of the free surface at each focal point. Simultaneously, a separate experiment was performed to acquire the Digital Particle Image Velocimetry (DPIV) images of the flow. A CCD camera was set up focusing on a small region of 0.5 cm × 0.3 cm. An argon-ion laser sheet was then shuttered with the camera signal to provide two instantaneous digital images with a known time difference between them. These images were then processed using the DPIV technique as presented by Willert and Gharib (1991) to provide velocity and vorticity fields of the flow.

Results

First, the free surface slope across the Reynolds ridge was measured. Figure 3 displays the data integrated to show the free surface deformation or height profile. This data is found to agree qualitatively with the slope profiles measured by Scott (1982). The velocity field in the vicinity of a Reynolds ridge, displaying the boundary layer beneath the surfactant film, for a free stream flow of 12 cm/s is shown in Fig. 4. (Note that the free surface is located at the top edge of the plots in both Figs. 4 and 6.) Extrapolated from this data, velocity profiles within the boundary layer at various downstream distances are presented in Figure 5. Notice the slight increase in steepness of the slope of the

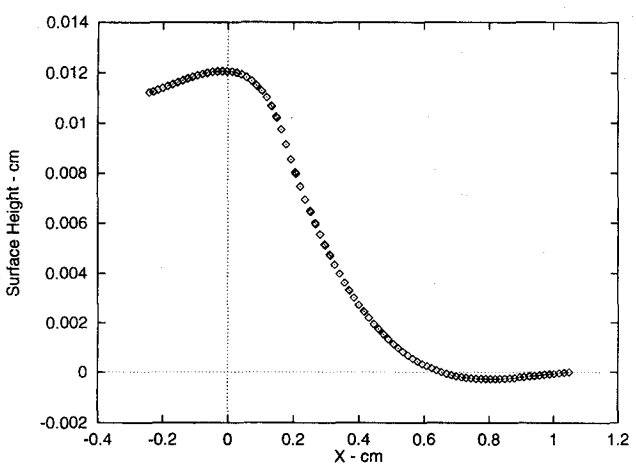

Fig. 3 Free surface height profile integrated from the slope measurement (measurement error <5 percent)

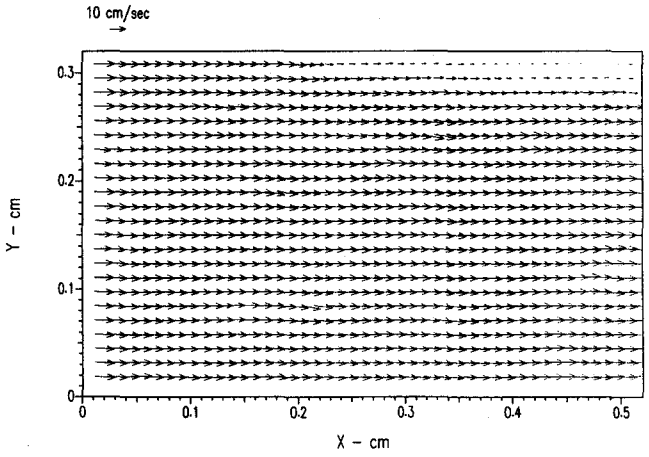

Fig. 4 Velocity field in the vicinity of a Reynolds ridge (measurement error <5 percent)

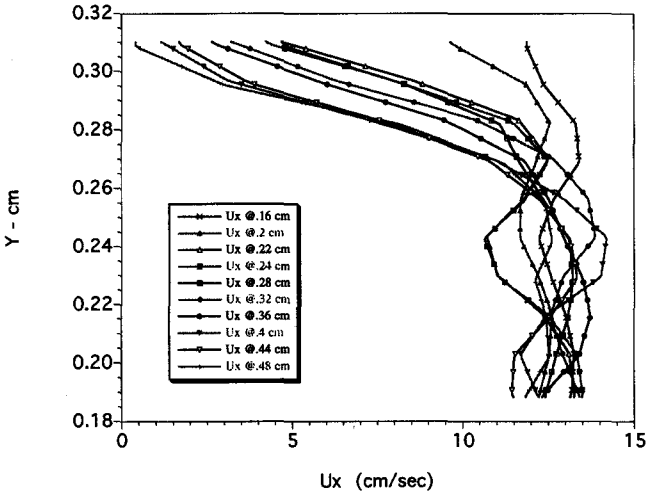

Fig. 5 Boundary layer profiles at various downstream distances (measurement error <5 percent)

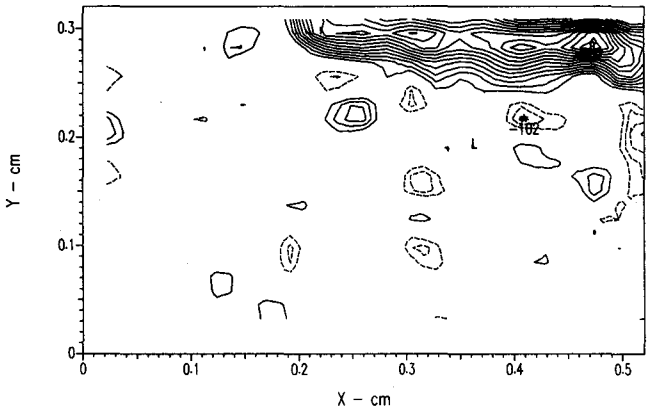

Fig. 6 Vorticity field in the vicinity of a Reynolds ridge (measurement error <10 percent)

profile near the free surface farther downstream. Other data obtained shows this trend to continue farther downstream of the ridge. In addition, the vorticity field calculated from the velocity data is shown in Fig. 6. Also extracted from the velocity data was the velocity profile along the free surface as shown in Fig.

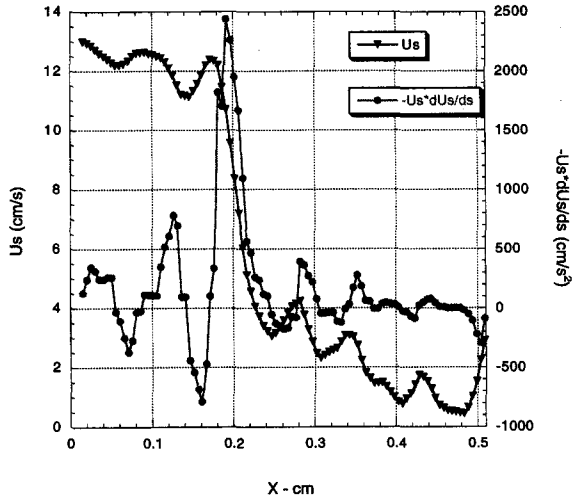

Fig. 7 Velocity and deceleration term (from Eq. (2)) profiles at the free surface (measurement error <5 percent)

7. From this, the deceleration term of Eq. (2) was calculated and is also presented in Fig. 7. The large fluctuation in the deceleration term upstream of the boundary layer is caused by to small fluctuations in the high velocity in this region. Still, one can see the large vorticity flux that occurs at the free surface because of the drastic drop in velocity that occurs on the ridge. Note how the flow initially decelerates ahead of the boundary layer but the peak in vorticity flux corresponds exactly to the point where the boundary layer begins.

Conclusions

From the above results, the magnitudes of the two terms in Eq. (2) may be estimated. From the theoretical calculations of the free surface profile by Harper and Dixon (1974), as well as the experimental results of Scott (1982) and those presented in Fig. 3, one can see that the angle θ over the deformation profile remains small such that the order of magnitude of the $g \cos \theta$ term is one or less. However, looking at Fig. 7, we see that the deceleration term reaches an order of magnitude of four. Therefore, the dominant source of vorticity in the vicinity of a Reynolds ridge is the deceleration of the flow at the free surface as it approaches the stagnant film. Notice too, it is in a small region of about 0.5 mm that this large vorticity flux occurs at the free surface. In other words it must be within the region where the surface tension gradient is located, as ahead of the film the water is considered clean and within the film itself no large gradients of surface tension subsist. It is interesting to note as well that this region occurs in the vicinity of the inflection point of the height profile of the ridge. It is at this point on the free surface as well that a slight downward component is detected in the velocity field. Thus all flow, but that right at the free surface moves down into the boundary layer beneath the film, while just at the free surface the flow is decelerated accounting for the change in curvature of the free surface. The vorticity generated by this deceleration is then convected downstream to form the boundary layer observed.

Also, the boundary layer profiles show evidence of approaching very small shear stress at the film as exhibited by the steepening of the boundary layer profiles farther downstream of the ridge. This agrees with the fact that there is no longer a large surface tension gradient at the free surface in the film to support that shear stress in the flow. These profiles exhibit a shape similar to those found near a flat plate in the presence of a pressure gradient. In further experiments we hope to gain a better understanding of this free surface boundary layer.

In addition, we plan to acquire simultaneous velocity field, free surface profile, and surface tension measurements near the

Reynolds ridge which will provide even more insight into the unique nature of this flow. But so far it has been determined that it is the boundary condition of the surface tension gradient at the free surface in the vicinity of a Reynolds ridge which causes the flow to dynamically conform, with a rapid deceleration over a small region, resulting in a large vorticity flux at the free surface.

Acknowledgments

We would like to thank Dana Dabiri for his help and advice while performing this work. This work was supported by ONR contract# N00014-94-1-0596. The National Science Foundation, and the Zonta International Amelia Earhart Fellowship Award have supported first author Amy Warncke towards her graduate work.

References

Gharib, M., 1992, "On Some Aspects of Near Surface Vortices,"

Gharib, M., and A. Weigand, 1995, "Experimental Studies of Vortex Disconnection and Connection at a Free Surface," submitted to *Journal of Fluid Mechanics.*

Harper, J. F. and Dixon, J. N., 1974, "The Leading edge of a Surface Film on Contaminated Flowing Water," *Proc. 5th Australian Conf. on Hydraulics and Fluid Mech.,* Christchurch, New Zealand, pp. 499–505.

Lugt, H. J., 1987, "Local Flow Properties at a Viscous Free Surface," *Physics of Fluids,* vol. 30, pp. 3647–3652.

Lugt, H. J., 1988, "Fundamental Viscous Flow Properties at a Free Surface," *Fluid Dynamics Transactions,* vol. 14, pp. 1–20.

Lundgren, T. S., 1988, "A Free Surface Vortex Method with Weak Viscous Effects," Mathematical Aspects of Vortex Dynamics," *Proceedings of the Workshop on Mathematical Aspects of Vortex Dynamics,* Leesburg, VA, pp. 68–79.

Rood, E. P., 1995, "Free-Surface Vorticity," Chapter 17 in *Fluid Vortices,* S. Green, ed., Kluwer Academic Publishing, Norwell, MA.

Roesgen, T., "Dynamic Surface Slope Measurements Using Microlens Arrays," to be published in *Experiment of Fluids.*

Sellin, R. H. J., 1968, *Nature,* Vol. 217, pp. 536–538.

Scott, S. C., 1982, "Flow Beneath a Stagnant Film on Water: the Reynolds ridge," *Journal of Fluid Mechanics,* vol. 116, pp. 283–296.

Willert, C., and M. Gharib, 1991, "Digital Particle Image Velocimetry," *Experiment in Fluids,* Vol. 10, pp. 181–183.

A Novel Pump for MEMS Applications

Mihir Sen,[1] Daniel Wajerski,[1] and Mohamed Gad-el-Hak[1]

We present a novel approach for pumping fluids in micromechanical applications at extremely low Reynolds numbers. It is based on the rotation of a cylinder placed asymmetrically in a narrow duct; the differential viscous resistance between the small and large gaps causes a net flow along the channel. We report on experiments using glycerin and several cm-scale prisms having circular, square, and rectangular cross-sections. The Reynolds number, based on cylinder size and angular velocity, varies in the range of 0.01–10. The flow is visualized using tracer particles. The flow generated depends on the geometrical parameters, but is proportional to the angular velocity of the cylinder. An average flow velocity that is about ten percent of the surface speed of the cylinder has been obtained.

Manufacturing processes that can create extremely small machines have been developed in recent years. Motors, electrostatic actuators, pneumatic actuators, valves, gears, and tweezers of about 10 μm size have been fabricated. These have been used as sensors for pressure, temperature, velocity, mass flow, or sound, and as actuators for linear and angular motions. Current usage ranges from airbags to blood analysis (O'Connor, 1992). There is considerable work under way to include other applications, one example being the micro-steam engine described by Lipkin (1993). Many of these new applications will need fluid to be pumped in a duct; at such small scales this is a challenge.

There have been several studies of microfabricated pumps. Some of them use nonmechanical effects. Ion-drag is used in electrohydrodynamic pumps (Bart et al., 1990; Richter et al., 1991; Fuhr et al., 1992); these rely on the electrical properties of the fluid and are thus not suitable for many applications. Valveless pumping by ultrasound has also been proposed (Moroney et al., 1991), but produces very little pressure difference.

It is important to emphasize that mechanical pumps based on conventional centrifugal or axial turbomachinery will not work at micromachine scales where the Reynolds numbers are typically small. Centrifugal forces are negligible and, furthermore, the Kutta condition through which lift is normally generated is invalid when inertial forces are vanishingly small. In general there are three ways in which mechanical micropumps can work:

(a) Positive-Displacement Pumps. These are mechanical pumps with a membrane or diaphragm actuated in a reciprocating mode and with unidirectional inlet and outlet valves. They work on the same physical principle as their larger cousins. Micropumps with piezoelectric actuators have been fabricated (Van Lintel et al., 1988; Esashi et al., 1989; Smits, 1990). Other actuators, such as thermopneumatic, electrostatic, electromagnetic or bimetallic, can be used. These exceedingly minute positive-displacement pumps require even smaller valves, seals and mechanisms, a not-too-trivial micromanufacturing challenge. In addition, there are long-term problems associated with wear or clogging and consequent leaking around valves. The pumping capacity of these pumps is also limited by the small displacement and frequency involved. Gear pumps are a different kind of positive-displacement device.

(b) Continuous, Parallel-Axis Rotary Pumps. A screw-type, three-dimensional device for low Reynolds numbers was proposed by Taylor (1972) for propulsion purposes and shown in his seminal film. It has an axis of rotation parallel to the flow direction implying that the powering motor must be submerged in the flow, the flow turned through an angle, or that complicated gearing would be needed.

(c) Continuous, Transverse-Axis Rotary Pumps. This is the class of machines that we propose here. We assert that a rotating body, asymmetrically placed within a duct, will produce a net flow due to viscous action. The axis of rotation can be perpendicular to the flow direction and the cylinder can thus be easily powered from outside a duct. A related viscous-flow pump was designed by Odell and Kovasznay (1971) for a water channel with density stratification. However, their design operates at a much higher Reynolds number and is too complicated for microfabrication.

Fluid flow at the micromachine level is complicated by issues such as interfacial forces, slip-flow and Knudsen number effects. To develop an operational viscous-flow micropump one must first demonstrate its working at the macroscale where these special effects are not important. Our purpose here is to show experimentally that viscous forces can indeed be used to pump fluid at low Reynolds numbers. Reynolds numbers representative of micromachine applications in air or water can be obtained with cm-size cylinders and with glycerin as the working

[1] Professor, Research Assistant, and Professor, respectively, Department of Aerospace and Mechanical Engineering, University of Notre Dame, Notre Dame, IN 46556. Professor Sen is a Mem. ASME; Professor Gad-el-Hak is a Fellow ASME.

Contributed by the Fluids Engineering Division of THE AMERICAN SOCIETY OF MECHANICAL ENGINEERS. Manuscript received by the Fluids Engineering Division February 26, 1996; revised manuscript received April 24, 1996. Associate Technical Editor: D. P. Telionis.